



A hydrogel derived from decellularized dermal extracellular matrix

Matthew T. Wolf^{a,c}, Kerry A. Daly^{b,c}, Ellen P. Brennan-Pierce^{a,c,1}, Scott A. Johnson^{b,c},
Christopher A. Carruthers^{a,c}, Antonio D'Amore^{a,c,e,f}, Shailesh P. Nagarkar^d, Sachin S. Velankar^d,
Stephen F. Badylak^{a,b,c,*}

^a Department of Bioengineering, University of Pittsburgh, 360B CNBIO, 300 Technology Drive, Pittsburgh, PA 15219, USA

^b Department of Surgery, University of Pittsburgh, Pittsburgh, PA 15261, USA

^c McGowan Institute for Regenerative Medicine, 450 Technology Drive, Suite 300, Pittsburgh, PA 15219, USA

^d Department of Chemical Engineering, University of Pittsburgh, 1249 Benedum Hall, 3700 O'Hara Street, Pittsburgh, PA 15261, USA

^e RiMed Foundation, Italy

^f DICGIM University of Palermo, Italy

ARTICLE INFO

Article history:

Received 14 May 2012

Accepted 22 June 2012

Available online 11 July 2012

Keywords:

ECM (extracellular matrix)

Hydrogel

Scaffold

Viscoelasticity

Surface topography

Cell viability

ABSTRACT

The ECM of mammalian tissues has been used as a scaffold to facilitate the repair and reconstruction of numerous tissues. Such scaffolds are prepared in many forms including sheets, powders, and hydrogels. ECM hydrogels provide advantages such as injectability, the ability to fill an irregularly shaped space, and the inherent bioactivity of native matrix. However, material properties of ECM hydrogels and the effect of these properties upon cell behavior are neither well understood nor controlled. The objective of this study was to prepare and determine the structure, mechanics, and the cell response *in vitro* and *in vivo* of ECM hydrogels prepared from decellularized porcine dermis and urinary bladder tissues. Dermal ECM hydrogels were characterized by a more dense fiber architecture and greater mechanical integrity than urinary bladder ECM hydrogels, and showed a dose dependent increase in mechanical properties with ECM concentration. *In vitro*, dermal ECM hydrogels supported greater C2C12 myoblast fusion, and less fibroblast infiltration and less fibroblast mediated hydrogel contraction than urinary bladder ECM hydrogels. Both hydrogels were rapidly infiltrated by host cells, primarily macrophages, when implanted in a rat abdominal wall defect. Both ECM hydrogels degraded by 35 days *in vivo*, but UBM hydrogels degraded more quickly, and with greater amounts of myogenesis than dermal ECM. These results show that ECM hydrogel properties can be varied and partially controlled by the scaffold tissue source, and that these properties can markedly affect cell behavior.

© 2012 Elsevier Ltd. All rights reserved.

1. Introduction

Injectable, *in situ* polymerizing hydrogels are being used with increasing frequency for biomedical applications such as cell delivery, drug delivery, and/or as a scaffold for reconstruction of injured tissue [1]. Injectable hydrogels have several desirable features for therapeutic applications including targeted delivery by minimally invasive techniques, ease of repeated delivery, ability to quickly fill an irregularly shaped space, and polymerization to form a support structure suitable for host cell infiltration and

remodeling. Most of the investigated injectable hydrogels have been synthetic polymers with defined structural, chemical, and mechanical properties finely tuned for a desired application. However, there have been a number of recent descriptions of injectable hydrogels derived from naturally occurring biologic materials with purported superior biocompatibility and bioactivity compared to their synthetic counterparts. Common constituents of biologic hydrogels include Type I collagen, hyaluronic acid, or other proteins such as laminin as found in Matrigel [2].

It has been shown that biologic scaffold materials composed of the extracellular matrix (ECM) of decellularized tissues can be partially digested with pepsin, solubilized, and polymerized *in situ* to form a hydrogel [3–10]. Intact ECM scaffold materials retain numerous molecular constituents found in the native tissue such as cell adhesion proteins, growth factors [11], and glycosaminoglycans and these materials support a constructive, site appropriate, remodeling response when implanted in a variety of anatomic sites

* Corresponding author. McGowan Institute for Regenerative Medicine, 450 Technology Drive, Suite 300, University of Pittsburgh, Pittsburgh, PA 15219, USA. Tel.: +1 412 235 5144; fax: +1 412 235 5110.

E-mail address: badylaks@upmc.edu (S.F. Badylak).

¹ Current address: School of Biomedical Engineering, Dalhousie University, Halifax, NS B3H 1W2, Canada.

including skeletal muscle [12–14], cardiac tissue [15], and the peripheral nervous system [16]. It is possible that a hydrogel formed from enzymatically degraded and solubilized ECM may maintain some of the biologic activity found in the intact ECM.

Unlike synthetic hydrogels, the physical and structural properties of ECM hydrogels have not been thoroughly characterized and the optimal methods for controlling these properties are not understood. Likely determinant factors of hydrogel properties include the tissue source and the decellularization methods used to prepare the ECM and the ECM concentration of the hydrogel. The objectives of the present study were: (1) to prepare a hydrogel from porcine dermal ECM, and (2) to compare the mechanical and material properties, *in vitro* cell growth characteristics, and *in vivo* remodeling properties of the dermal ECM (D-ECM) hydrogel with a previously described ECM hydrogel derived from porcine urinary bladder matrix (UBM) [3].

2. Materials and methods

2.1. Overview

ECM hydrogels were prepared from decellularized porcine dermis and urinary bladder and evaluated *in vitro* for mechanical behavior, biochemical composition, and cell response. D-ECM and UBM gels were then evaluated in a skeletal muscle injury model *in vivo* for host response and remodeling characteristics. Six independent batches of D-ECM and UBM were prepared from separate ECM isolations. All animal experiments were conducted in accordance with University of Pittsburgh Institutional Animal Care and Use Committee (IACUC) regulations and guidelines.

2.2. Preparation of D-ECM and UBM hydrogels

D-ECM was prepared as previously described [17]. Full thickness skin was harvested from market weight (approximately 110 kg) pigs. The subcutaneous fat, connective tissue, and epidermis were removed by mechanical delamination to isolate the dermal layer, and then stored at -80°C . Dermis was then thawed and treated with the following solutions under constant agitation on an orbital shaker at 300 RPM: 0.25% trypsin (Thermo Fisher Scientific, Waltham, MA), for 6 h, three 15 min washes of deionized water, 70% ethanol for 10 h, 3% H_2O_2 for 15 min, two 15 min washes of deionized water, 1% Triton X-100 in 0.26% EDTA/0.69% Tris for 6 h with a fresh change for an additional 16 h, three 15 min washes of deionized water, 0.1% peracetic acid/4% ethanol for 2 h, two 15 min washes of PBS, and two 15 min washes of deionized water.

UBM was evaluated in parallel to D-ECM, and was prepared as previously described [18]. In brief, porcine urinary bladders from market weight pigs were harvested, and the urothelial, serosal, and muscular layers were removed by mechanical delamination. The remaining tissue consisted of intact basement membrane and tunica propria, which was rinsed with deionized water and then treated with 0.1% peracetic acid/4% ethanol on an orbital shaker at 300 RPM for 2 h. The UBM was then rinsed twice with PBS for 15 min each followed by two 15 min rinses in deionized water.

Both D-ECM and UBM were frozen and lyophilized for use in hydrogel preparation [3,6]. In brief, lyophilized ECM scaffolds were powdered using a Wiley Mill and filtered through a 40 mesh screen. The comminuted ECM was then enzymatically digested in a solution of 1 mg/ml porcine pepsin (Sigma–Aldrich, St. Louis, MO) in 0.01 N HCl under a constant stir rate for 72 h at room temperature. ECM pepsin digest stock solutions of 10 mg ECM/ml (dry wt.) were frozen until use in subsequent experiments. Gelation was induced by neutralizing the pH and salt concentration of the pepsin digest at 4°C followed by warming to 37°C . Neutralization was accomplished by the addition of one-tenth the digest volume of 0.1 N NaOH, one-ninth the digest volume of $10\times$ PBS, and then diluting to the desired final ECM concentration with $1\times$ PBS while on ice. The neutralized digest (pre-gel) was then placed in a non-humidified incubator heated to 37°C for 1 h, after which, a hydrogel had formed. ECM concentrations of 2, 4, 6, and 8 mg/ml were prepared. Pre-gel was also injected through a syringe and 18G needle to subjectively determine injectability.

2.3. Evaluation of surface ultrastructure and hydrogel fiber orientation

The surface topology of D-ECM and UBM gels was examined using scanning electron microscopy, and the fiber network characteristics quantified using a previously developed image analysis algorithm ($n = 6$) run on MATLAB software (Mathworks, Natick, MA) [19]. ECM hydrogels at 2, 4, 6 and 8 mg/ml ECM concentrations were fixed in cold 2.5% (v/v) glutaraldehyde (Electron Microscopy Sciences, Hatfield, PA) in PBS for 24 h followed by three 30 min $1\times$ PBS washes. Gels were dehydrated in a graded series of alcohol (30, 50, 70, 90, 100% ethanol in PBS) for 45 min per wash, and then left in 100% ethanol overnight at 4°C . After 3 additional

45 min changes in 100% ethanol, hydrogels were slowly critical point dried (Leica EM CPD030 Critical Point Dryer, Leica Microsystems, Buffalo Grove, IL). After drying, gels were sputter coated (Sputter Coater 108 Auto, Cressington Scientific Instruments, Watford, UK) with a 4.5 nm thick gold/palladium alloy coating and imaged with a scanning electron microscope (JEOL JSM6330F, JEOL Ltd., Peabody, MA). A complete set of fiber network descriptors was collected from SEM images of each ECM hydrogel including: fiber alignment, node density (number of fiber intersections per μm^2), and fiber diameter. Fiber alignment was described through the normalized orientation index where 0% represents a randomly organized (isotropic) network, while 100% represents a completely aligned (anisotropic) network. Porosity was described through the mean of the pore size histogram (μm^2). Automated extraction of these fiber architectural features was achieved with an algorithm, which has been previously described in detail [19]. Briefly, the SEM image is digitally processed by a cascade of steps including equalization with a 3×3 median filter, local thresholding through the Otsu method, thinning, smoothing, morphological operators, skeletonization, binary filtering for Delaunay network refinement, and ultimately the detection of fiber network architecture and its descriptors.

2.4. ECM hydrogel rheology

The rheological characteristics of D-ECM and UBM hydrogels were determined with a rheometer (AR2000, TA instruments, New Castle, DE) operating with a 40 mm parallel plate geometry. The temperature was controlled within 0.1°C using a Peltier plate. Typical rheometer gap was 450–750 μm . ECM digests were pH neutralized on ice and were immediately loaded onto the rheometer plate pre-cooled to 10°C . Mineral oil was spread along the edge (i.e. the free surface of the hydrogel) to minimize evaporation. After loading, the steady shear viscosity was measured by applying a stress of 1 Pa at a frequency of 0.159 Hz. The temperature was then increased to 37°C to induce gelation and a small amplitude oscillatory strain of 0.5% was imposed to track the gelation kinetics. After complete gelation, a creep test (1 Pa for 20 s) was performed to verify that there was no slip between the ECM hydrogels and rheometer plates. A small oscillatory frequency sweep experiment was then conducted for D-ECM conducted at 0.5% strain in the frequency range from 0.079 Hz to 6.33 Hz.

2.5. Turbidimetric gelation kinetics

The gelation kinetics of ECM hydrogels were evaluated turbidimetrically and kinetic parameters derived for comparisons ($n = 4$). Neutralized liquid D-ECM and UBM pre-gel solutions at 4, 6, and 8 mg/ml concentrations were prepared on ice. For each concentration, 100 μl /well was added in triplicate in 96-well plates and read spectrophotometrically in a plate reader (Spectramax M2, Molecular Devices, Sunnyvale, CA) pre-heated to 37°C . Absorbance at 405 nm was measured every 2 min for 60 min. The readings were then scaled from 0 (at time 0) to 100% (at maximum absorbance) according to Equation (1) where NA is the normalized absorbance, A is the absorbance at a given time, A_0 is the initial absorbance, and A_{max} is the maximum absorbance.

$$\text{NA} = \frac{A - A_0}{A_{\text{max}} - A_0} \quad (1)$$

The time to half gelation ($t_{1/2}$) was defined as the time to 50% absorbance, the gelation rate (S) was defined as the slope of the linear region of the gelation curve, and the lag time (t_{lag}) was defined as the intercept of the linear region of the gelation curve with 0% absorbance.

2.6. Collagen and sulfated GAG content of ECM pepsin digests

D-ECM and UBM pepsin digests were diluted and assayed for soluble, triple helical collagen content using the Sircol Collagen Assay (Biocolor Ltd., Carrickfergus, United Kingdom) per the manufacturer's instructions ($n = 6$). A pepsin buffer solution was used as the negative control and subtracted from the signal. Similarly, pH neutralized digests were analyzed for sulfated GAG concentration using the Blyscan Sulfated Glycosaminoglycan Assay (Biocolor Ltd.) per the manufacturer's instructions ($n = 5$).

2.7. *In vitro* cell culture and viability

In vitro cell growth on the surface or within the gel bulk was characterized for 6 and 8 mg/ml D-ECM and UBM gels. These concentrations were selected because of the different mechanical and structural properties observed between these concentrations. The cell types evaluated were NIH 3T3 fibroblasts (CRL-1658, ATCC, Manassas, VA) and C2C12 myoblasts (CRL-1772, ATCC). C2C12 myoblasts were cultured in both growth and fusion conditions. NIH 3T3 and C2C12 myoblast growth media was Dulbecco's Modified Eagle Medium (DMEM; Sigma–Aldrich) supplemented with 10% fetal bovine serum (FBS) and 1% penicillin/streptomycin (Thermo Fisher Scientific). C2C12 myoblasts were differentiated into myotubes using fusion medium consisting of DMEM supplemented with 2% horse serum (Thermo Fisher Scientific) and 1% penicillin/streptomycin for an additional 2 days after 7 days of

culture in growth medium. C2C12 myoblasts were examined at the 6 mg/ml concentration only.

One-half (0.5) ml hydrogels were prepared in 1.38 cm inner diameter stainless steel annular rings at 6 and 8 mg/ml concentrations for cell seeding experiments. Cells were seeded on the surface of hydrogels by depositing 1 ml of cell suspension on the fully formed hydrogel while inside of a seeding ring for a final seeding density of 5×10^5 cells/cm². Cells were allowed to attach for 16 h, then the seeding rings were removed and media changed. Cells were seeded within the gel bulk by adding 32 μ l of concentrated cell suspension per ml of neutralized liquid pre-gel solution for a final cell concentration of 1×10^6 cells/ml. Cells were thoroughly mixed in the pre-gel and then brought to 37 °C for 45 min inside of the seeding rings, during which time the hydrogel had formed around the cells. The seeding rings were removed and 5 ml of media added. Media was changed every 3 days for both seeding methods.

Cell viability on the surface of both 3T3 fibroblast and C2C12 myoblast seeded hydrogels was determined after 7 days in culture using the Live/Dead assay (Invitrogen, Carlsbad, CA). C2C12 myoblasts after culture in fusion media were also evaluated. Gels were incubated for 15 min in 1 μ M calcein-AM and 1 μ M ethidium homodimer-1 at 37 °C, washed in PBS, and imaged by fluorescent methods within 1 h. C2C12 cells were imaged using confocal microscopy (Leica DMI 4000B, Leica Microsystems) to more accurately assess cell morphology. Histologic analysis was conducted after 3 and 7 days of culture, after which time hydrogels were fixed in 10% neutral buffered formalin, embedded in paraffin, sectioned, and stained with Masson's Trichrome. C2C12 myoblasts were also evaluated for viability and histologic appearance after 2 additional days of fusion conditions.

2.8. Cell infiltration quantification of ECM hydrogels

The infiltration of 3T3 fibroblasts seeded on the surface of 6 and 8 mg/ml ECM hydrogels was quantified using histologic methods after 3 and 7 days in culture ($n = 3$ from two independent batches of each ECM). Two or three fields (100 \times) of hydrogel histologic cross sections spanning the entire gel surface were imaged, and the cell infiltration distance from the surface quantified. Ten measurements of the maximum cell infiltration distance were taken at evenly spaced intervals across each image using ImageJ software (National Institute of Health, Bethesda, MD) and the values were averaged. The total hydrogel thickness was determined to normalize infiltration as percent of the hydrogel thickness. The maximum infiltration distance was defined as the greatest distance cells migrated from the surface (μ m) for each hydrogel.

2.9. Contraction of ECM hydrogels

ECM hydrogel contraction after cells had been seeded within the bulk was quantified using macroscopic image analysis ($n = 6$ –12, from two independent batches of each ECM). Free-floating ECM hydrogels were imaged inside their respective wells in 6-well plates after 12 h, 1, 3, and 7 days in culture. Gels were fixed and imaged for histologic appearance after 3 and 7 days in culture. The top surface area of hydrogels was determined by tracing the border using ImageJ software compared to a reference within each image, and then converted to percent of the unseeded hydrogel area. Unseeded ECM hydrogels at both ECM concentrations remained in identical culture conditions and for the same timepoints as cell seeded hydrogels.

2.10. In vivo host response to ECM hydrogels in a site of muscle injury

The *in vivo* compatibility and remodeling of ECM hydrogels were evaluated in a rat partial thickness abdominal wall defect model as previously described [12,14]. A 1×1 cm defect was created via excision of the internal and external oblique muscles, leaving the *transversalis fascia* and peritoneum intact. One ml aliquots of 8 mg/ml (the concentration with greatest mechanical integrity) D-ECM and UBM hydrogels were prepared in 1.2 cm \times 1.2 cm molds using sterile buffer solutions. ECM hydrogels were placed within the defect, and non-degradable polypropylene marker sutures placed at the four corners of the defect. Unrepaired defects were also prepared as a control group. After 3, 7, 14, or 35 days, rats were sacrificed and the defect site and adjacent abdominal wall were explanted and fixed in 10% neutral buffered formalin. The tissue was then embedded in paraffin, sectioned, and stained with Masson's Trichrome. Low powered fields (40 \times) of the histologic cross sections were imaged, and the gel thickness quantified with ImageJ software.

Sections were immunolabeled for the pan macrophage marker CD68. After deparaffinization, sections were subjected to epitope retrieval in 10 mM citrate buffer (pH = 6) at 95–100 °C for 20 min. Sections were washed and blocked with 1% bovine serum albumin (BSA)/10% horse serum in Tris-buffered saline (TBS) for 1 h at room temperature and then incubated with mouse anti-rat CD68 antibody (1:100, clone ED1, MCA341R, AbD Serotec, Raleigh, NC) diluted in 1% BSA in TBS overnight at 4 °C. Sections were washed, followed by quenching of endogenous peroxidase activity with 0.3% (v/v) hydrogen peroxide solution in TBS for 15 min at room temperature. Sections were then washed and incubated in a HRP conjugated goat anti-mouse IgG secondary antibody (1:200, Vector, Burlingame, CA) diluted in 1% BSA in TBS solution for 1 h at room temperature. Sections were washed and exposed to a diaminobenzidine substrate (DAB Peroxidase Substrate Kit, SK4100, Vector)

until appropriate staining developed. Slides were counterstained with hematoxylin, dehydrated, cover slipped, and imaged.

Muscle cell phenotypes were confirmed via immunolabeling for fast and slow myosin heavy chain as previously described [12–14]. Slides were deparaffinized followed by epitope retrieval in 0.1 mM EDTA at 95–100 °C for 25 min followed by 0.1% trypsin/0.1% calcium chloride (w/v) at 37 °C for 10 min. Endogenous peroxidase activity was quenched after incubation in a 0.3% (v/v) hydrogen peroxide solution in TBS for 10 min. Sections were blocked with 2% normal horse serum/1% BSA in TBS for 30 min at room temperature and then labeled for mouse anti-slow myosin heavy chain (1:1000, clone NOQ7.5.4D, M8421, Sigma–Aldrich) for 40 min at room temperature followed by rinsing in TBS. Sections were incubated in a biotinylated goat anti-mouse IgG secondary antibody (1:200, Vector) diluted in blocking solution for 1 h at room temperature followed by rinsing in TBS. Sections were incubated in the Vectastain ABC reagent (Vectastain Elite ABC Kit, Vector) for 30 min at room temperature and then developed with a diaminobenzidine substrate (ImmPact DAB, Vector). Sections were incubated in blocking solution for 10 min followed by incubation in alkaline phosphatase conjugated mouse anti-fast myosin heavy chain (1:200, clone MY-32, A4335, Sigma) diluted in blocking solution for 1 h. Color was developed by staining with alkaline phosphatase (Red Alkaline Phosphatase Kit, SK-5100, Vector), dehydrated, and cover slipped.

Myogenesis was quantified at the 35 day timepoint by determining the total cross sectional area of myosin heavy chain positive cells within the defect borders. Mosaic images spanning the entire defect were obtained, and each myosin heavy chain positive cell border was traced and the area quantified with ImageJ software. A blinded observer distinguished the location of the defect border from the intact native tissue and identified myogenesis by the presence of centrally located nuclei within cells that were also positive for myosin heavy chain.

2.11. Statistical analysis

All statistical analyses were performed using SPSS software (IBM SPSS Statistics, IBM, Armonk, NY). Hydrogel fiber orientation, rheology, gelation kinetics, *in vitro* cell infiltration, *in vitro* contraction, *in vivo* thickness, and *in vivo* myogenesis were analyzed using a one-way analysis of variance (ANOVA) with a post-hoc Tukey test. The total soluble collagen and sulfated GAG content were analyzed using a student's *t*-test. Significance for all statistical analyses was defined as $p < 0.05$. All values are reported as the mean \pm standard error of the mean.

3. Results

3.1. Macroscopic appearance of ECM hydrogels

Hydrogels were successfully prepared from both D-ECM (Fig. 1A–D) and UBM (Fig. 1E–H) scaffolds at concentrations ranging from 2 to 8 mg/ml and were found to be injectable through a syringe and 18G needle. Macroscopically, the higher ECM concentration 6–8 mg/ml hydrogels had the most rigid structure with defined edges, and could be handled and manipulated with forceps. As ECM concentration decreased to 2–4 mg/ml, hydrogels became softer with rounded edges.

3.2. Evaluation of surface ultrastructure and hydrogel fiber orientation

Scanning electron microscopy of the gel surface showed qualitatively that both D-ECM (Fig. 1E–H) and UBM (Fig. 1M–P) hydrogels possessed a randomly oriented fibrillar structure, which was subsequently characterized quantitatively [19]. Visual inspection of algorithm output showed accurate automatic detection of the fiber network for both D-ECM and UBM hydrogels at multiple concentrations (Supplemental Figure 1). D-ECM fiber diameter and pore size had a non-linear decrease with increasing concentration from $0.094 \pm 0.005 \mu$ m and $0.128 \pm 0.017 \mu$ m² at the 2 mg/ml concentration to $0.069 \pm 0.005 \mu$ m and $0.059 \pm 0.001 \mu$ m² at 8 mg/ml concentration, respectively. However, fiber diameter and pore size of UBM hydrogels were found to be independent of ECM concentration within the range of 2–8 mg/ml at $0.074 \pm 0.004 \mu$ m and $0.112 \pm 0.005 \mu$ m, respectively (Fig. 1Q–R). D-ECM node density exponentially increased with increasing concentration from 5.73 ± 0.69 nodes/ μ m² to 10.08 ± 0.22 nodes/ μ m² while the fiber intersection density of UBM hydrogels again showed no obvious

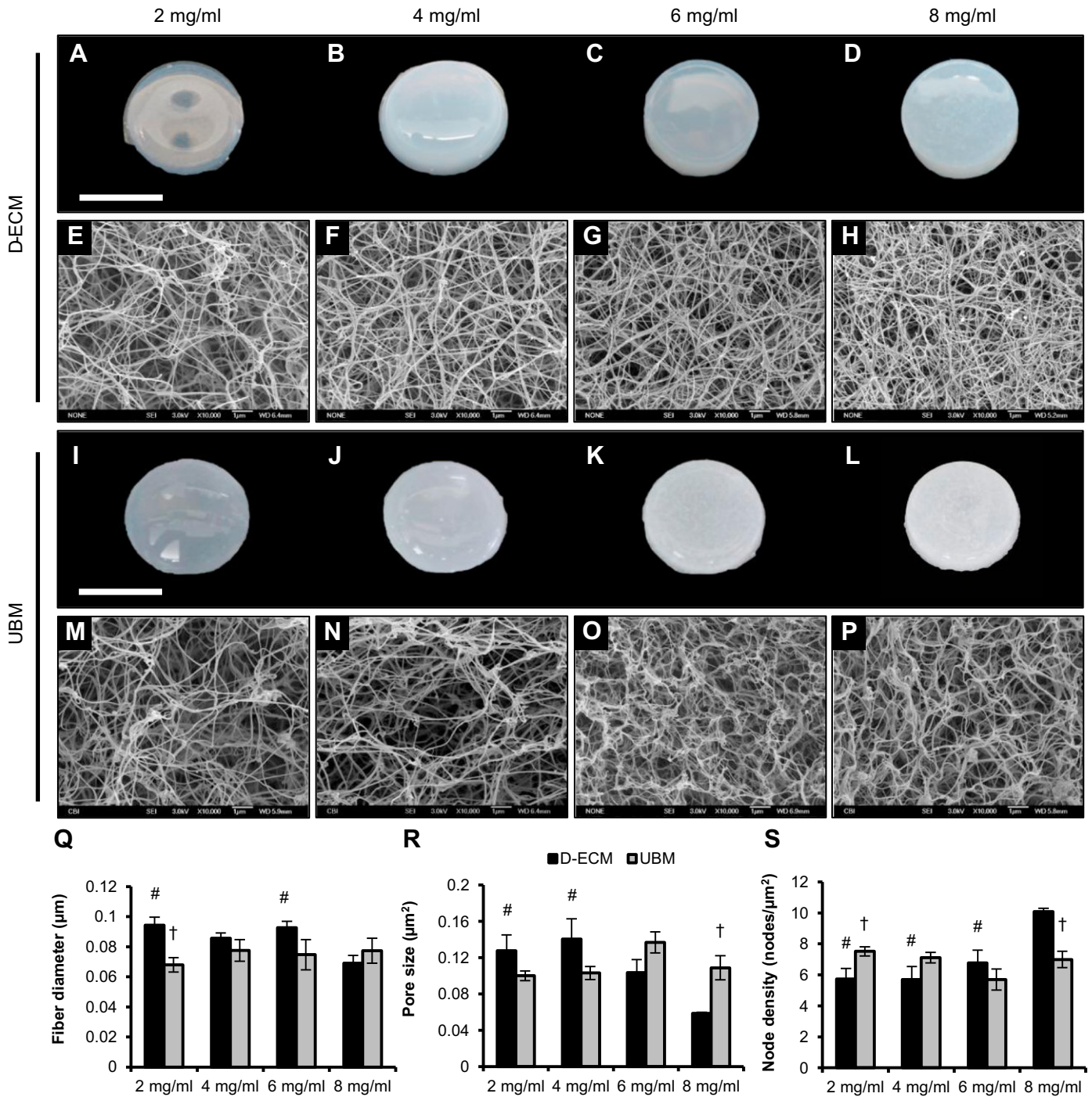


Fig. 1. Macroscopic appearance, surface topology, and fiber network analysis of ECM hydrogels. ECM pepsin digests were pH neutralized and injected into 1.38 cm inner diameter rings at 37 °C for 1 h. Macroscopic images were obtained and hydrogels were processed for scanning electron microscopy. Scanning electron micrographs were obtained at 10,000 \times magnification for D-ECM and UBM hydrogels prepared at ECM concentrations of 8, 6, 4, and 2 mg/ml. SEM images were analyzed using an automated fiber tracking algorithm to determine the average fiber diameter, pore size, and node density of ECM hydrogels at each concentration. # denotes significance from the 8 mg/ml concentration of the same ECM type and † denotes significance between D-ECM and UBM at the same concentration ($p < 0.05$). Scale bar for macroscopic images represents 1 cm.

trend with concentration (Fig. 1S). The networks of both ECM hydrogels lacked any angular alignment with a normalized orientation index close to 0%, confirming the qualitative assessment.

3.3. ECM hydrogel rheology

The rheological characteristics of ECM hydrogels were determined using a parallel plate rheometer. The storage (G') and loss

modulus (G'') of ECM hydrogels increased after ECM pepsin digests were neutralized and the temperature was raised from 10 to 37 °C. Solid like behavior was confirmed because the storage modulus was greater than the loss modulus by approximately a factor of 10 after gelation. Both D-ECM (Fig. 2A) and UBM (Fig. 2B) showed an increase in rate of gelation with increasing concentration. The final steady state storage modulus of fully formed D-ECM hydrogels increased rapidly and non-linearly with concentration, while UBM

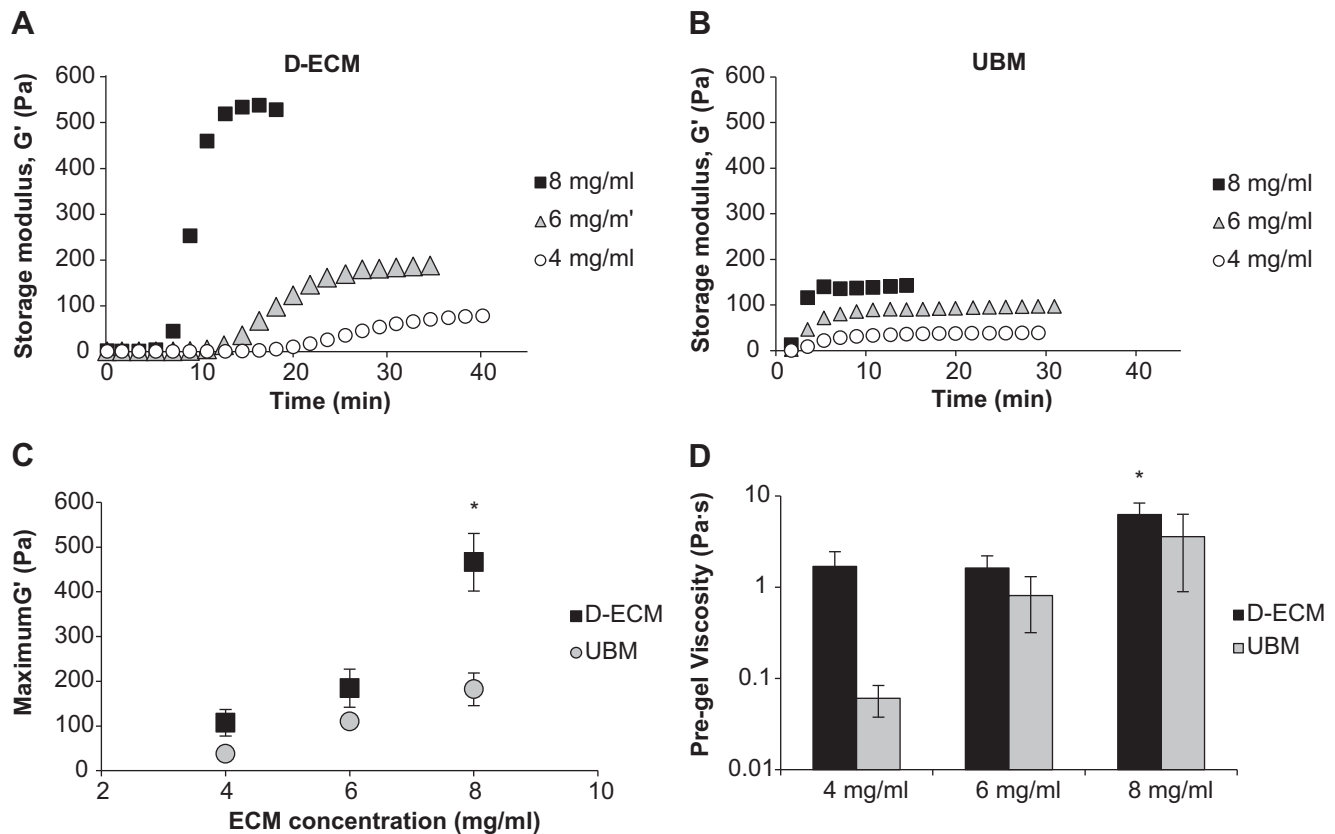


Fig. 2. Rheological characterization of ECM hydrogels. Representative curves of the gelation kinetics of D-ECM (A) and UBM (B) hydrogels at ECM concentrations of 8, 6, and 4 mg/ml were determined by monitoring changes in the storage modulus (G') after inducing gelation. The maximum storage modulus after complete gelation for each hydrogel was plotted as a function of ECM concentration (C). * denotes significance between D-ECM at 8 mg/ml from all other data points. The initial steady shear viscosity of the neutralized digest was determined under constant stress (D) prior to gelation. * denotes significance between D-ECM at 8 mg/ml and UBM at 4 mg/ml only ($p < 0.05$).

hydrogels had a linear increase based on the three concentrations tested. Both D-ECM and UBM hydrogels had the highest modulus at the 8 mg/ml ECM concentration wherein D-ECM and UBM had a storage modulus of 466.5 ± 64.3 and 182.2 ± 36.5 Pa, respectively (Fig. 2C). The viscosities of D-ECM and UBM pre-gel (neutralized digest prior to gelation) ranged between 0.02 and 10.08 Pa s, and the viscosity tended to be higher for D-ECM than UBM. The average viscosity of D-ECM pre-gel at 8 mg/ml was greater than UBM at 4 mg/ml at 6.27 ± 2.08 and 0.10 ± 0.06 Pa s, respectively (Fig. 2D). Post gelation creep analysis of 8 mg/ml D-ECM and UBM hydrogels showed a viscoelastic strain profile (Supplemental Figure 2A–B) characterized by a rapid initial strain increase with creep ringing, followed by a slower increase and plateau. The creep modulus (Supplemental Figure 2C–D) for both D-ECM and UBM hydrogels quickly reached steady state modulus values that were similar to the storage modulus found during oscillatory strain with no evidence of slip between the samples and rheometer plates. The frequency response of D-ECM to an oscillatory strain was evaluated (Supplemental Figure 2E) after creep analysis. The storage modulus of D-ECM hydrogel showed no dependence on frequency at any concentration, and was greater at the 8 mg/ml ECM concentration than 6 or 4 mg/ml for all frequencies tested.

3.4. Turbidimetric gelation kinetics

The turbidimetric gelation kinetics of D-ECM (Fig. 3A) and UBM (Fig. 3B) hydrogels was characterized spectrophotometrically over a range of concentrations and the gelation parameters (lag time, gelation rate, and time to 50% gelation) quantified. ECM hydrogel

formation began after a lag period (t_{lag}), and occurred more quickly for UBM and at higher concentrations. The lag time for UBM at 8 mg/ml was 11.1 ± 2.5 min compared to 24.5 ± 1.2 min for D-ECM at 4 mg/ml (Supplemental Figure 3A). The time to 50% gelation ($t_{1/2}$) followed the trend of increased time for D-ECM compared to UBM and lower concentrations, but was not statistically significant (Supplemental Figure 3B). Gelation rate (S) tended to be greater for D-ECM than UBM, but was not strongly dependent on concentration (Supplemental Figure 3C).

3.5. Collagen and sulfated GAG content of ECM pepsin digests

The soluble collagen content of D-ECM was 0.85 ± 0.04 mg collagen/mg ECM (dry wt.), which was greater than the 0.58 ± 0.03 mg collagen/mg ECM found for UBM at the same total ECM concentration (Fig. 4A). Conversely, the total sulfated GAG content of D-ECM digests were much lower in D-ECM than UBM with 1.11 ± 0.06 and 3.20 ± 0.06 μ g GAG/mg ECM (dry wt.), respectively (Fig. 4B).

3.6. In vitro cell culture and viability

Almost all NIH 3T3 fibroblasts cultured on the surface and within the bulk of both D-ECM and UBM hydrogels at 6 and 8 mg/ml concentrations were viable (green cytoplasm without red nuclei) after 7 days (Supplemental Figure 4). Fibroblasts were confluent on the surface with a cobblestone morphology, and there were no differences in viability based on ECM hydrogel type, concentration, or cell seeding method. Histologic analysis of

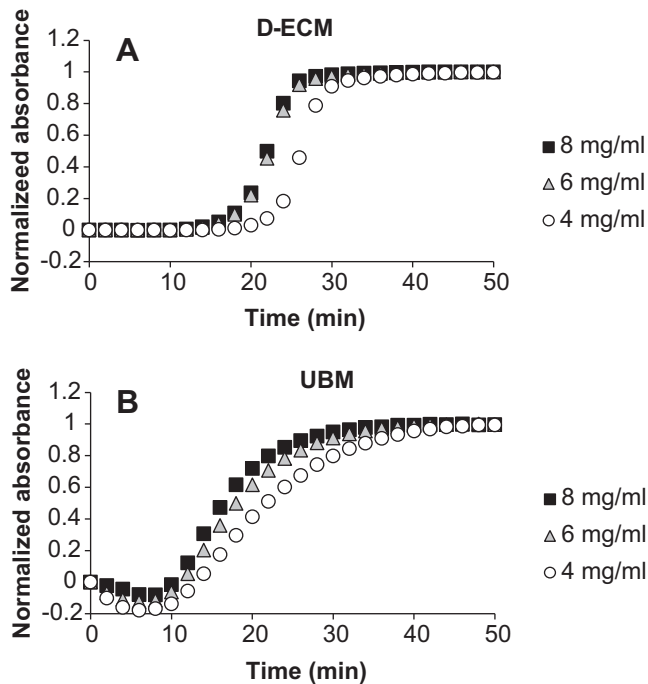


Fig. 3. Turbidimetric gelation kinetics of ECM hydrogels. Representative curves of D-ECM (A) and UBM (B) hydrogels at ECM concentrations of 8, 6, and 4 mg/ml. ECM pepsin digests were pH neutralized and added to the wells of a 96-well plate at 37 °C to induce gelation. The absorbance at 405 nm was measured at 2 min intervals and normalized between 0 (the initial absorbance) and 1 (the maximum absorbance).

fibroblasts seeded on the surface of ECM hydrogels showed a confluent monolayer of cells at 3 and 7 days, and varying degrees of infiltration (quantified in Section 3.7). Fibroblasts seeded within hydrogels were distributed throughout the hydrogel (Supplemental Figure 5), with a higher cell density at and near the surface of the hydrogel compared to the center. Hydrogels with greater contraction (and a corresponding decrease in cross sectional area) showed a greater cell density, but overall a similar number of cells.

C2C12 myoblasts were seeded both on the surface and within the bulk of D-ECM and UBM hydrogels at 6 mg/ml ECM concentration. The Live/Dead assay showed that the majority of cells were viable when cultured on the surface or within the bulk of both ECM types (Fig. 5B,D,F,H,J,L). However, cells appeared more confluent on D-ECM hydrogels than UBM as seen via histology and the Live/Dead assay for both seeding methods. Both D-ECM and UBM hydrogels showed cells distributed throughout the entire volume when the

cells were seeded within the hydrogel bulk (Fig. 5A,C). By 7 days of culture, C2C12 myoblasts had begun to fuse into large diameter multinucleated myotubes when seeded on the surface of D-ECM hydrogels, and to a far lesser extent on UBM hydrogels where there were fewer, smaller elongated cell structures present (Fig. 5E–H). After 2 days in fusion media, only myoblasts seeded on the surface of D-ECM hydrogels had developed into mature myotubes with a radial alignment (Fig. 5I–J). Myoblasts seeded on or within UBM hydrogels, or within D-ECM hydrogels did not form large myotubes.

3.7. Cell infiltration quantification of ECM hydrogels

NIH 3T3 fibroblasts infiltrated both D-ECM and UBM hydrogels when seeded on the surface of hydrogels at ECM concentrations of 6 and 8 mg/ml (Fig. 6A–H), and all ECM hydrogel types and concentrations showed an increase in infiltration over time between 3 and 7 days. Cells reached a maximum infiltration depth of $1312.6 \pm 103.0 \mu\text{m}$ for UBM hydrogels at the 6 mg/ml concentration after 7 days, which was significantly different from the D-ECM hydrogels that infiltrated $843.8 \pm 86.0 \mu\text{m}$. Increased infiltration into UBM hydrogels compared to D-ECM was also observed for the 8 mg/ml concentration after 7 days, with 1265.4 ± 142.4 and $741.6 \pm 136.9 \mu\text{m}$, respectively (Fig. 6I). During culture, it was observed that there was hydrogel contraction, therefore the infiltration measurements were normalized as a percent of infiltration through the hydrogel thickness (Fig. 6J). The normalized values again showed an increase in infiltration between 3 and 7 days for both D-ECM and UBM hydrogels at both 6 and 8 mg/ml concentrations, and there was greater infiltration into UBM hydrogels than D-ECM hydrogels at the 6 mg/ml ECM concentration after 7 days. UBM hydrogels were infiltrated $68.6 \pm 9.7\%$ of the hydrogel thickness at the 6 mg/ml concentration, which was greater than the $43.7 \pm 6.9\%$ observed for the 8 mg/ml concentration after 7 days.

3.8. Contraction of ECM hydrogels

ECM hydrogel contraction increased over time between 12 h and 7 days in culture, the rate of which was dependent on both the ECM type and ECM concentration (Fig. 7A–E). The unseeded hydrogel area did not change regardless of ECM type, concentration, or time point. Hydrogel contraction quantification (Fig. 7F) showed that D-ECM hydrogels at an ECM concentration of 8 mg/ml contracted the least at $87.9 \pm 1.3\%$ of the initial area after 7 days. D-ECM contracted to a greater extent at the 6 mg/ml concentration than the 8 mg/ml to $49.6 \pm 10.8\%$ on the initial area by 7 days. UBM hydrogels at both 6 and 8 mg/ml were similar and showed the most contraction after 7 days at $15.2 \pm 0.6\%$ and $12.7 \pm 1.5\%$, respectively. However, the rate of contraction differed for UBM hydrogels at 6 and 8 mg/ml concentrations. UBM hydrogels at the lower 6 mg/ml concentration contracted more rapidly than the 8 mg/ml concentration, with $24.6 \pm 0.5\%$ and $43.7 \pm 3.0\%$, respectively after 3 days in culture.

3.9. In vivo host response to ECM hydrogels in a site of muscle injury

D-ECM and UBM hydrogels at an 8 mg/ml ECM concentration were implanted in a rat partial thickness abdominal wall defect and evaluated after 3, 7, 14, and 35 days of implantation. D-ECM and UBM hydrogels degraded quickly over the 35 day time course, based on histologic appearance from Masson's Trichrome stained cross sections (Fig. 8A–D & Supplemental Figure 7A–D). ECM hydrogels were faintly blue staining, and filled the entirety of the defect at early timepoints. UBM hydrogels were significantly thinner than D-ECM hydrogels after 3, 7, and 14 days, but by 35

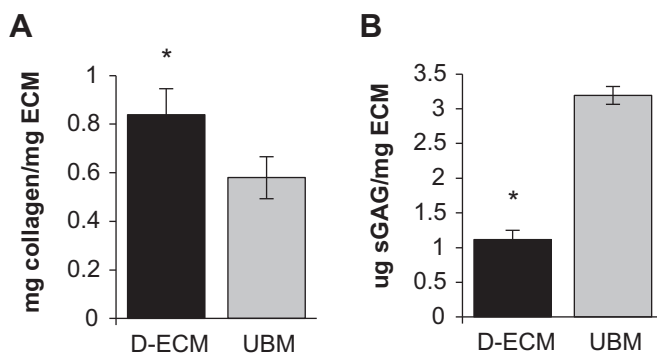


Fig. 4. Biochemical composition of ECM hydrogels. Soluble collagen (A) and sulfated GAG (B) content of D-ECM and UBM pepsin digests were determined using the Sircol and Blyscan assays, respectively. * denotes significance between ECM types.

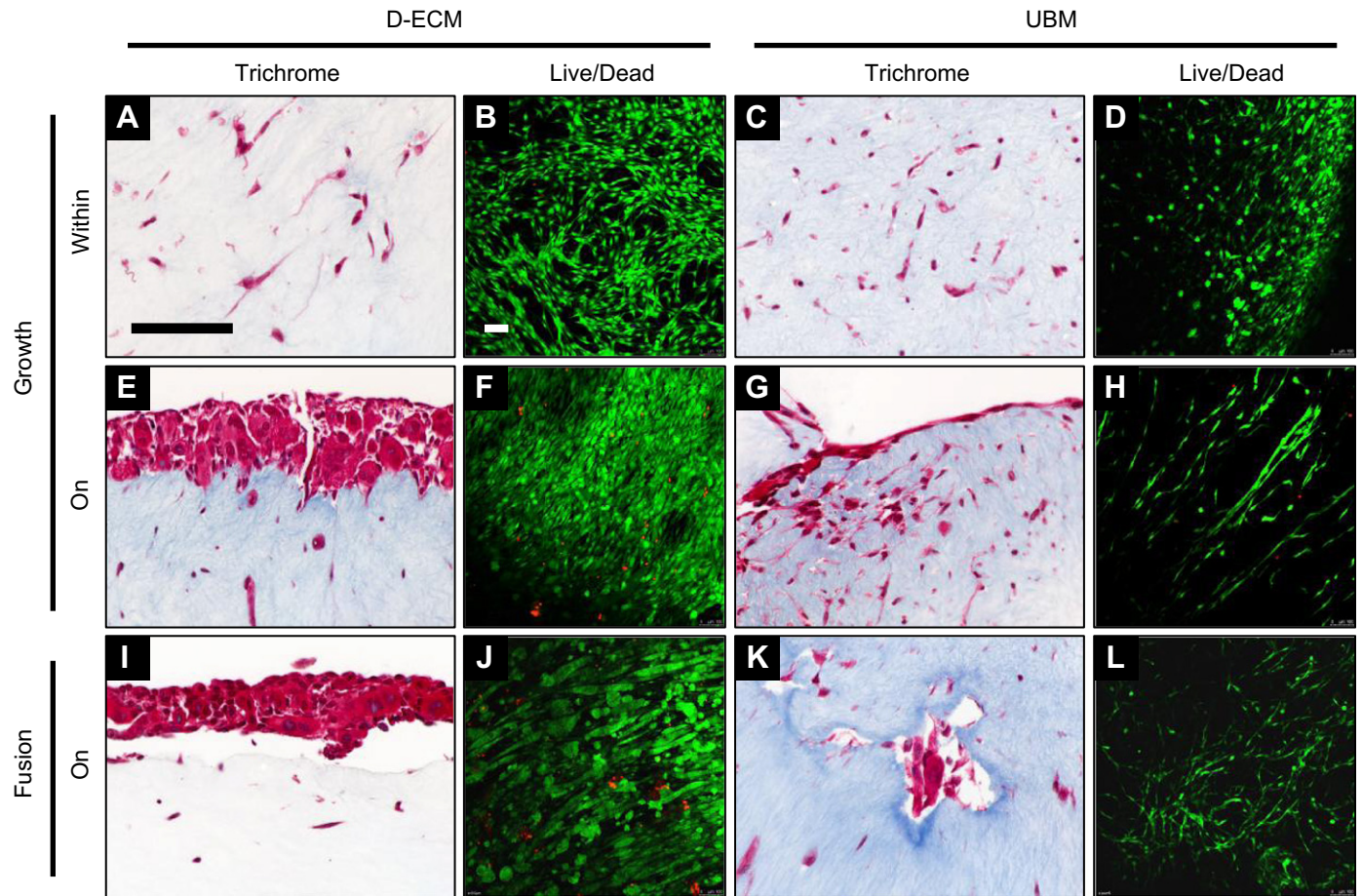


Fig. 5. Myogenic potential of ECM hydrogels in vitro. C2C12 myoblasts were cultured on the surface and within D-ECM and UBM hydrogels in growth and fusion conditions. C2C12 myoblasts were evaluated via histologic analysis of Masson's Trichrome stained cross sections and Live/Dead staining of the hydrogel surface for viable cells (green) and dead cell nuclei (red) imaged with confocal microscopy. C2C12 myoblasts were cultured for 7 days in growth media or for 7 days in growth media followed by 3 additional days in low serum fusion media to induce myotube formation. Scale bars represent 100 μ m. (For interpretation of the references to color in this figure legend, the reader is referred to the web version of this article.)

days, both D-ECM and UBM had almost completely degraded as determined by histologic quantification (Fig. 8E). The macroscopic appearance of the defect area also confirmed the slower degradation kinetics for D-ECM (Supplemental Figure 6) where the D-ECM hydrogel was visible up to 14 days and UBM was only visible for 7 days.

Both ECM hydrogels were completely infiltrated throughout the entire hydrogel thickness by CD68+ cells within 3 days of implantation (Fig. 8F–G). CD68+ cells continued to populate the hydrogels at all timepoints, and remained in the remodeling tissue after the hydrogel had degraded (Fig. 8H–I & Supplemental Figure 7E–H). The remodeling defect area also showed signs of myogenesis at 35 days, with large fusing myoblasts with centrally located nuclei and scattered islands of fast or slow myosin heavy chain positive cells (Fig. 8J–K). The myosin heavy chain positive cells were most densely located near the defect borders, though occasionally populated the center of the defect. Total muscle cell area was quantified based on morphology and myosin heavy chain positive staining. UBM hydrogels induced a greater amount of myogenesis than an unrepaired defect alone (Fig. 8L).

4. Discussion

Porcine dermal ECM can be solubilized and subsequently induced to form an injectable hydrogel under physiologically

relevant pH, salt concentration, and temperature that is capable of supporting viable cell growth. D-ECM hydrogels were evaluated for structural, mechanical, and *in vitro* cell response characteristics; all of which were found to be ECM concentration dependent. Compared to hydrogels composed of UBM, which is derived from a different tissue and prepared by a different decellularization method, D-ECM possesses different and distinct physical and biologic properties. Relative to UBM, D-ECM hydrogels have increased mechanical stability, soluble collagen content, fibril density, and *in vitro* myogenesis potential. UBM hydrogels have greater amounts of GAGs, allow greater cell infiltration/contraction *in vitro*, and promote greater myogenesis *in vivo*. These results indicate that the physical and biologic properties of an ECM hydrogel can be altered and at least partially controlled by the specific ECM scaffold utilized and the ECM concentration.

Potential advantages of ECM hydrogels for therapeutic applications include the robust biologic activity from constituent matrix molecules, and ease of delivery using minimally invasive techniques to fill irregular spaces. Numerous synthetic polymer hydrogels have been developed for injectability, but lack notable biologic activity without the addition of bioactive molecules such as exogenous growth factors or peptides [2,20,21]. Biologic scaffolds prepared from decellularized tissues can promote and facilitate a constructive and site appropriate remodeling response *in vivo* as shown in various pre-clinical studies [12–16,22]. Although the

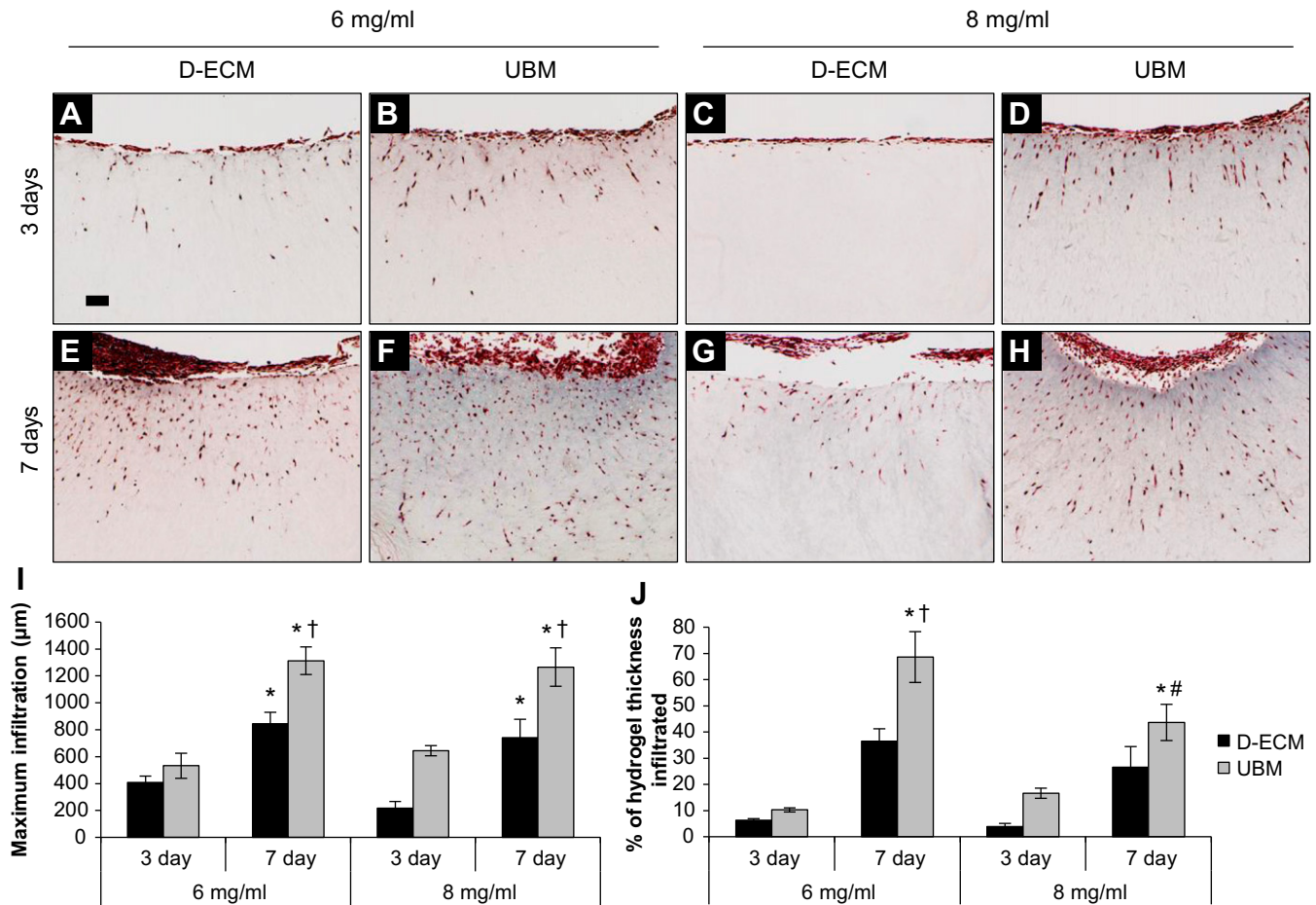


Fig. 6. Cell infiltration into ECM hydrogels. NIH 3T3 fibroblasts were seeded on the surface of D-ECM (A,E,C,G) and UBM (B,D,F,H) hydrogels at ECM concentrations of 6 and 8 mg/ml after 3 and 7 days of culture. The distance infiltrated from the surface was quantified via histologic analysis of Masson's Trichrome stained cross sections. The maximum distance infiltrated from the surface by any cell was determined (I) as well as the average infiltration across the entire hydrogel (J). * denotes significance between days 3 and 7 (for the same ECM type/concentration), † denotes significance between D-ECM and UBM (within the same timepoint/concentration), and # denotes significance between the 8 and 6 mg/ml concentrations (at the same ECM type/timepoint). Scale bar represents 100 µm.

mechanisms of this phenomenon are only partially understood, modulation of the host immune response [23], recruitment of endogenous stem and progenitor cells [24], and rapid and complete scaffold degradation play important roles. It is unknown whether these events are mediated by ECM surface topographical features, specific structural ligands, released bioactive molecules, and/or other mechanisms. The present study in which the matrix is enzymatically degraded, solubilized, and then repolymerized suggests that the constitutive molecules of the ECM at least play an important role.

Host cells, particularly macrophages, actively participate in the degradation of implanted intact ECM scaffolds, and both macrophage participation and scaffold degradation are essential for constructive remodeling [12,23]. Degradation of intact ECM scaffolds promotes the release of matricryptic molecules; that is oligopeptide and oligosaccharide derivatives of the native ECM [25]. These matricryptic molecules possess a variety of bioactive properties including recruitment of endogenous stem and progenitor cells, antimicrobial activity, and angiogenic effects, among others [26–28]. *In vitro* pepsin degraded and solubilized ECM scaffolds have been used as a model for investigating the effects ECM degradation products. Pepsin digests of UBM have mitogenic and chemoattractant effects on dermal progenitor keratinocytes, endothelial cells, and stem cells *in vitro* [29–32].

In vivo degradation of intact ECM scaffolds have been shown to produce chemoattractant molecules for progenitor cells [24]. Likewise, UBM pepsin digests promote the accumulation of multipotent stem cells in a mouse digit amputation model [33,34]. When applied to pre-clinical models of cardiac injury, ECM degradation products increase vascularization and cardiomyocyte number [35]. The specific type and profile of biologic activities are highly dependent on the tissue type from which the ECM is isolated [36], processing method [17], and other factors such as age of the tissue [37]. D-ECM scaffold processing methods have been previously optimized to maximize the quantity of retained tissue specific molecules such as growth factors and GAGs and supporting *in vitro* cell growth, while simultaneously removing effectively all of the cell components [17]. In short, an ECM hydrogel represents a potentially potent mixture of signaling molecules that modulate the recipient remodeling response when placed *in vivo*, and both the D-ECM and UBM scaffolds have been optimized for this purpose.

ECM hydrogels have been previously developed from various tissue sources including liver [36], dermis [6,38–40], adipose tissue [9,40,41], urinary bladder [3,42], small intestine [10], cardiac tissues [7,8,35], skeletal muscle [4], and central nervous system tissues [5] using different methods of soluble ECM isolation such as high salt protein extraction or pepsin digestion. These studies show a range

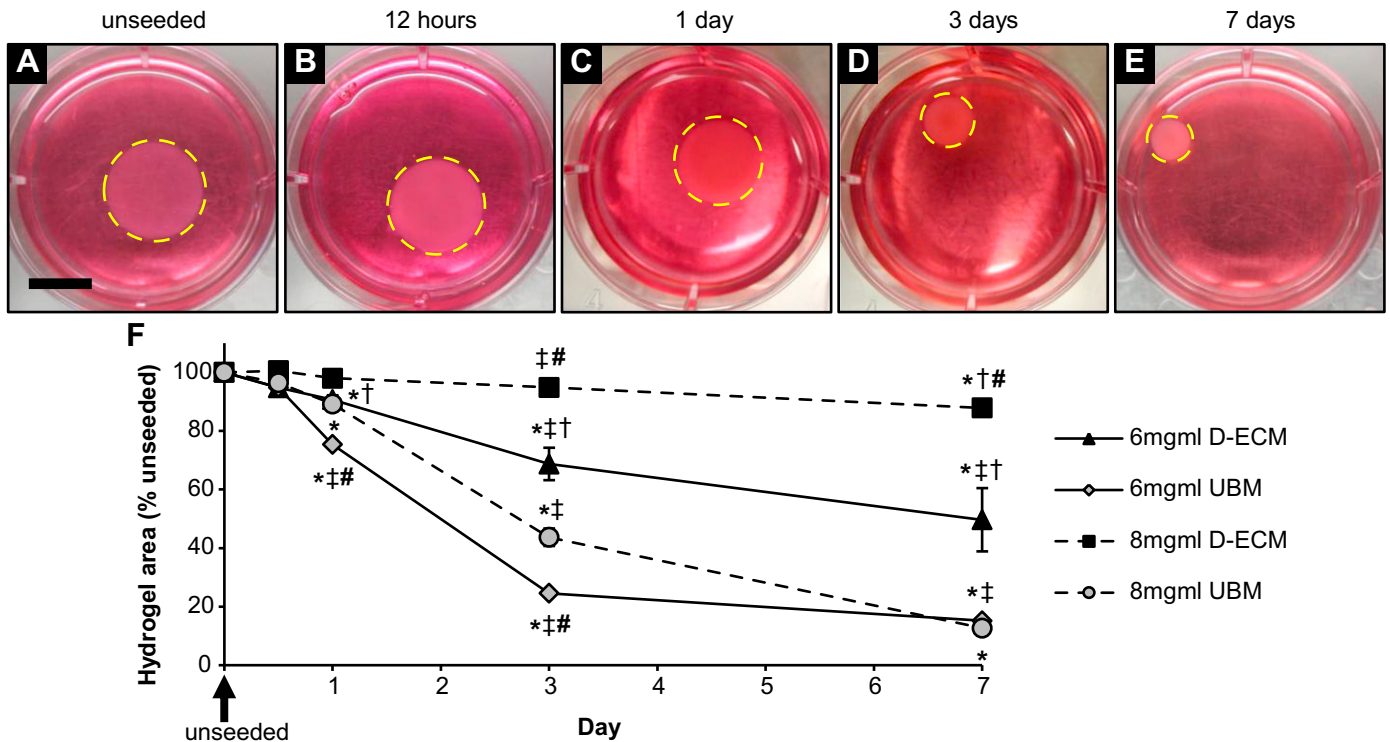


Fig. 7. Contraction of ECM hydrogels. NIH 3T3 fibroblasts were cultured within D-ECM and UBM hydrogels at ECM concentrations of 8 and 6 mg/ml, and imaged macroscopically after 12 h, 1 day, 3 days, and 7 days in culture (representative images of 6 mg/ml UBM with the hydrogel border traced with a dotted yellow line, A–E). The hydrogel contraction was quantified from these images and is expressed as % area of the unseeded control for each ECM type/concentration/timepoint. * denotes significance from the unseeded control, † denotes significance from the previous timepoint for an ECM type/concentration, ‡ denotes significance between D-ECM and UBM at the same timepoint/concentration, and # denotes significance between concentration of the same ECM type/timepoint. Scale bar represents 1 cm. (For interpretation of the references to color in this figure legend, the reader is referred to the web version of this article.)

of hydrogel properties, and the present study provides a systematic characterization of hydrogels derived from two dissimilar tissues and decellularization methods. The differences in hydrogel properties from different ECM scaffolds are likely due to variations in composition. D-ECM has a greater fraction of soluble triple helical collagens, which are the probable fibril forming elements of an ECM hydrogel, compared to UBM. The total collagen content of the ECM digest, which includes insoluble, crosslinked collagen, was not quantified. GAG content also was also greater in UBM than D-ECM, which may directly affect gel properties [43]. Additionally, SEM imaging and analysis showed that D-ECM hydrogels have a higher fiber node density than UBM and a higher storage modulus. There is a strong correlation between fiber node density and mechanical strength consistent with descriptions of fibrous networks [44], and which may have implications on *in vivo* cell behavior. The compositional variation may be attributed to the inherent differences between the native tissues and the decellularization method used to prepare them.

In vitro cell behavior is greatly affected by the mechanical environment of the substrate on which they are attached; therefore, ECM hydrogel structure and mechanical properties may also influence the cell response [45–50]. UBM hydrogels are more readily infiltrated and contracted by fibroblasts *in vitro* than D-ECM at the same ECM concentration, which might be expected based upon the greater interfiber distance (pore size) and lower storage modulus of UBM. However, the observed responses logically represent the net effect of hydrogel structure, mechanical properties, and the biologic activity of specific degradation products. Cell infiltration of a scaffold and fibroblast mediated contraction is especially important in certain types of wound healing.

ECM hydrogel properties affect the host remodeling response in a skeletal muscle defect model *in vivo*. D-ECM hydrogels, similar to the *in vitro* experiments, are less readily infiltrated than UBM, and are degraded more slowly. As previously shown for intact ECM scaffolds, CD68+ cells (monocytes/macrophages) are a critical component of the remodeling process [23] and constitute the majority of infiltrating cells in both ECM hydrogels in the present study. These cells are likely contributors to hydrogel degradation. ECM scaffold degradation *in vivo* is also associated with increased polarization towards an M2 phenotype, which in turn has been implicated in promoting constructive remodeling [51]. Both D-ECM and UBM hydrogels showed evidence of site appropriate constructive remodeling, specifically early myogenesis events in the defect region. Contrary to the *in vitro* result, remodeled UBM hydrogels *in vivo* promote greater myogenesis than D-ECM, a result that emphasizes the complex host/material interaction that occurs *in vivo* compared to *in vitro*.

Understanding the physical and biologic properties of ECM hydrogels may provide the opportunity to more effectively utilize an ECM hydrogel construct for specific therapeutic applications, where characteristics such as degradation kinetics or mechanical stability are of importance. Currently, few methods have been described to adjust the physical properties of ECM hydrogels, which include alterations in salt concentration or chemical cross linking [52,53]. This study shows that the tissue source, decellularization method, and ECM concentration are all variables that affect the desired hydrogel properties. A potentially important consideration for choosing the ECM source for a hydrogel application is the tissue specificity of the source ECM. Recent studies suggest that some tissues respond more favorably to an ECM scaffold derived from homologous tissue [22,36].

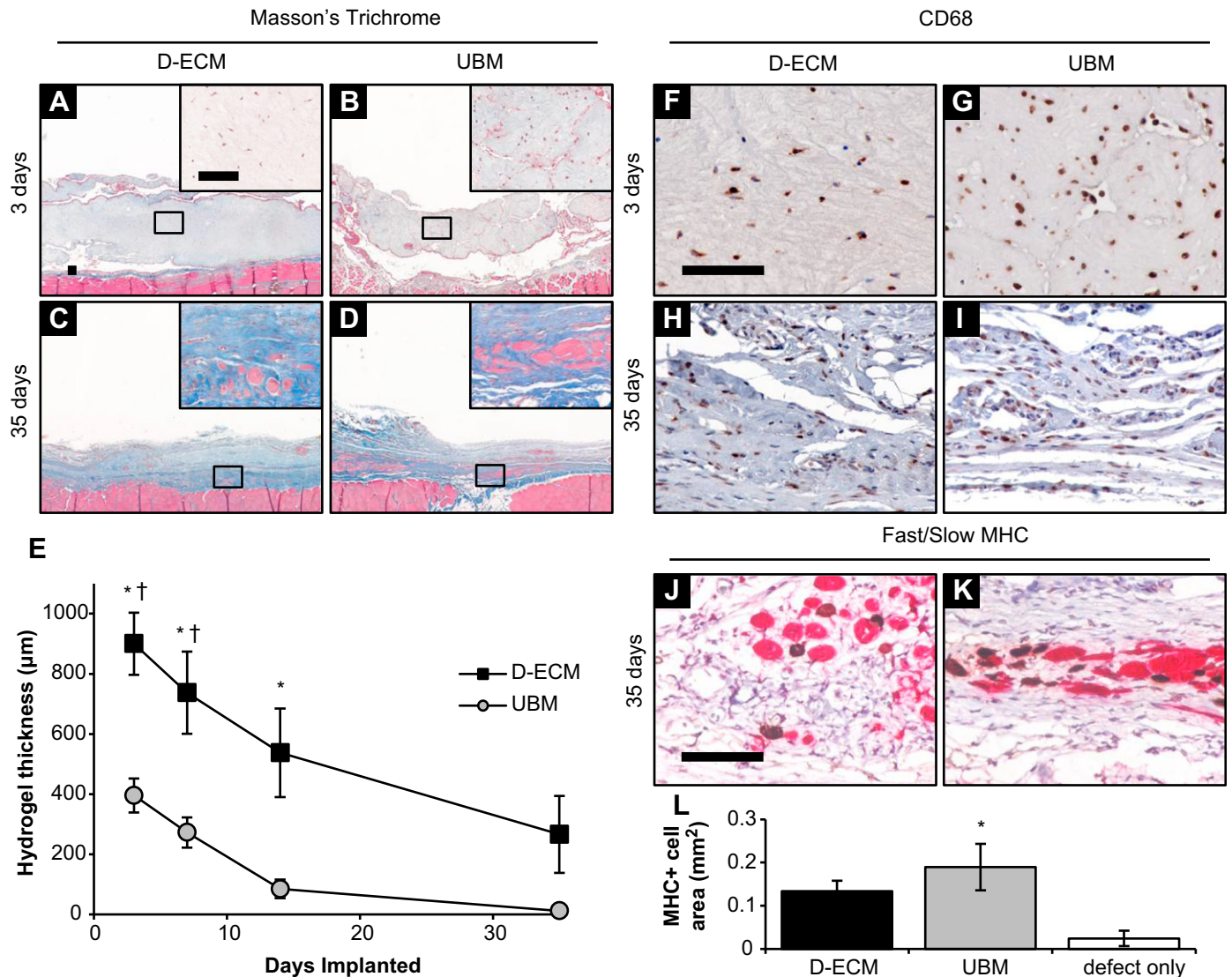


Fig. 8. *In vivo* response to ECM hydrogels in a rat skeletal muscle defect. D-ECM and UBM hydrogels were prepared at an ECM concentration of 8 mg/ml and then implanted in a 1×1 cm partial thickness rat abdominal wall defect for 3, 7, 14, or 35 days. The histologic appearance of Masson's Trichrome and CD68 stained sections were determined after 3 and 35 days showing $40\times$ and $400\times$ (inset) magnifications. The hydrogel thickness was quantified at each timepoint from the histologic cross sections. Myogenesis was determined via immunolabeling for slow (brown) and fast (red) myosin heavy chain (MHC) after 35 days of hydrogel implantation, and the total MHC positive cell area within the defect was quantified and compared to an unrepaired control. * denotes significance from the 35 day timepoint, and † denotes significance between D-ECM and UBM within a timepoint. Scale bars represent 100 µm. (For interpretation of the references to color in this figure legend, the reader is referred to the web version of this article.)

5. Conclusions

Porcine dermal ECM hydrogel can be prepared from an intact scaffold, and has distinct structural, mechanical, and biologic properties. ECM hydrogel properties can be manipulated by such factors as the source tissue from which the hydrogel was prepared and the final ECM concentration, and it may occur in a non-linear fashion. ECM hydrogel biologic properties *in vitro* and the skeletal muscle remodeling *in vivo* suggest that the constituent ECM molecules released from the intact scaffold during *in vitro* degradation remain active in the hydrogel architecture.

Acknowledgments

Funding for this study was provided through a grant from the National Institutes of Health (NIH 5R01 AR054940-03) and by C.R.

Bard, Inc. Matthew Wolf was partially supported by the NIH-NHLBI training grant (T32-HL76124-6) entitled "Cardiovascular Bioengineering Training Program" through the University of Pittsburgh Department of Bioengineering. Christopher Carruthers was partially supported by the National Science Foundation (NSF) Graduate Research Fellowship. Shailesh Nagarkar was partially supported by a grant from the National Science Foundation (NSF 0932901). The authors would like to thank Deanna Rhoads and the McGowan Histology Center for histologic section preparation and the center for Biologic Imaging at the University of Pittsburgh for access to imaging facilities.

Appendix A. Supplementary material

Supplementary material associated with this article can be found, in the online version, at <http://dx.doi.org/10.1016/j.biomaterials.2012.06.051>.

References

- [1] Van Vlierberghe S, Dubruel P, Schacht E. Biopolymer-based hydrogels as scaffolds for tissue engineering applications: a review. *Biomacromolecules* 2011;12(5):1387–408.
- [2] Tibbitt MW, Anseth KS. Hydrogels as extracellular matrix mimics for 3D cell culture. *Biotechnol Bioeng* 2009;103(4):655–63.
- [3] Freytes DO, Martin J, Velankar SS, Lee AS, Badyal SF. Preparation and rheological characterization of a gel form of the porcine urinary bladder matrix. *Biomaterials* 2008;29(11):1630–7.
- [4] DeQuach JA, Mezzano V, Miglani A, Lange S, Keller GM, Sheikh F, et al. Simple and high yielding method for preparing tissue specific extracellular matrix coatings for cell culture. *PLoS One* 2010;5(9):e13039.
- [5] DeQuach JA, Yuan SH, Goldstein LS, Christman KL. Decellularized porcine brain matrix for cell culture and tissue engineering scaffolds. *Tissue Eng Part A* 2011;17(21–22):2583–92.
- [6] Hong Y, Huber A, Takanari K, Amoroso NJ, Hashizume R, Badyal SF, et al. Mechanical properties and in vivo behavior of a biodegradable synthetic polymer microfiber-extracellular matrix hydrogel biohybrid scaffold. *Biomaterials* 2011;32(13):3387–94.
- [7] Seif-Naraghi SB, Salvatore MA, Schup-Magoffin PJ, Hu DP, Christman KL. Design and characterization of an injectable pericardial matrix gel: a potentially autologous scaffold for cardiac tissue engineering. *Tissue Eng Part A* 2010;16(6):2017–27.
- [8] Singelyn JM, DeQuach JA, Seif-Naraghi SB, Littlefield RB, Schup-Magoffin PJ, Christman KL. Naturally derived myocardial matrix as an injectable scaffold for cardiac tissue engineering. *Biomaterials* 2009;30(29):5409–16.
- [9] Young DA, Ibrahim DO, Hu D, Christman KL. Injectable hydrogel scaffold from decellularized human lipoaspirate. *Acta Biomater* 2011;7(3):1040–9.
- [10] Okada M, Payne TR, Oshima H, Momoi N, Tobita K, Huard J. Differential efficacy of gels derived from small intestinal submucosa as an injectable biomaterial for myocardial infarct repair. *Biomaterials* 2010;31(30):7678–83.
- [11] Voytik-Harbin SL, Brightman AO, Kraine MR, Waisner B, Badyal SF. Identification of extractable growth factors from small intestinal submucosa. *J Cell Biochem* 1997;67(4):478–91.
- [12] Valentin JE, Turner NJ, Gilbert TW, Badyal SF. Functional skeletal muscle formation with a biologic scaffold. *Biomaterials* 2010;31(29):7475–84.
- [13] Turner NJ, Yates Jr AJ, Weber DJ, Qureshi IR, Stolz DB, Gilbert TW, et al. Xenogeneic extracellular matrix as an inductive scaffold for regeneration of a functioning musculotendinous junction. *Tissue Eng Part A* 2010;16(11):3309–17.
- [14] Wolf MT, Daly KA, Reing JE, Badyal SF. Biologic scaffold composed of skeletal muscle extracellular matrix. *Biomaterials* 2012;33(10):2916–25.
- [15] Quarti A, Nardone S, Colaneri M, Santoro G, Pozzi M. Preliminary experience in the use of an extracellular matrix to repair congenital heart diseases. *Interact Cardiovasc Thorac Surg* 2011;6:569–72.
- [16] Nagao RJ, Lundy S, Khaing ZZ, Schmidt CE. Functional characterization of optimized acellular peripheral nerve graft in a rat sciatic nerve injury model. *Neuro Res* 2011;33(6):600–8.
- [17] Reing JE, Brown BN, Daly KA, Freund JM, Gilbert TW, Hsiong SX, et al. The effects of processing methods upon mechanical and biologic properties of porcine dermal extracellular matrix scaffolds. *Biomaterials* 2010;31(33):8626–33.
- [18] Freytes DO, Badyal SF, Webster TJ, Geddes LA, Rundell AE. Biaxial strength of multilaminated extracellular matrix scaffolds. *Biomaterials* 2004;25(12):2353–61.
- [19] D'Amore A, Stella JA, Wagner WR, Sacks MS. Characterization of the complete fiber network topology of planar fibrous tissues and scaffolds. *Biomaterials* 2010;31(20):5345–54.
- [20] Silva AK, Richard C, Bessodes M, Scherman D, Merten OW. Growth factor delivery approaches in hydrogels. *Biomacromolecules* 2009;10(1):9–18.
- [21] Stile RA, Healy KE. Thermo-responsive peptide-modified hydrogels for tissue regeneration. *Biomacromolecules* 2001;2(1):185–94.
- [22] Badyal SF, Weiss DJ, Caplan A, Macchiarini P. Engineered whole organs and complex tissues. *Lancet* 2012;379(9819):943–52.
- [23] Valentin JE, Stewart-Akers AM, Gilbert TW, Badyal SF. Macrophage participation in the degradation and remodeling of extracellular matrix scaffolds. *Tissue Eng Part A* 2009;15(7):1687–94.
- [24] Beattie AJ, Gilbert TW, Guyot JP, Yates AJ, Badyal SF. Chemoattraction of progenitor cells by remodeling extracellular matrix scaffolds. *Tissue Eng Part A* 2009;15(5):1119–25.
- [25] Davis GE, Bayless KJ, Davis MJ, Meininger GA. Regulation of tissue injury responses by the exposure of matrix-cryptic sites within extracellular matrix molecules. *Am J Pathol* 2000;156(5):1489–98.
- [26] Brennan EP, Reing J, Chew D, Myers-Irvin JM, Young EJ, Badyal SF. Antibacterial activity within degradation products of biological scaffolds composed of extracellular matrix. *Tissue Eng* 2006;12(10):2949–55.
- [27] Adair-Kirk TL, Senior RM. Fragments of extracellular matrix as mediators of inflammation. *Int J Biochem Cell Biol* 2008;40(6–7):1101–10.
- [28] Mott JD, Werb Z. Regulation of matrix biology by matrix metalloproteinases. *Curr Opin Cell Biol* 2004;16(5):558–64.
- [29] Brennan EP, Tang XH, Stewart-Akers AM, Gudas LJ, Badyal SF. Chemoattractant activity of degradation products of fetal and adult skin extracellular matrix for keratinocyte progenitor cells. *J Tissue Eng Regen Med* 2008;2(8):491–8.
- [30] Reing JE, Zhang L, Myers-Irvin J, Cordero KE, Freytes DO, Heber-Katz E, et al. Degradation products of extracellular matrix affect cell migration and proliferation. *Tissue Eng Part A* 2009;15(3):605–14.
- [31] Tottey S, Corselli M, Jeffries EM, Londono R, Peault B, Badyal SF. Extracellular matrix degradation products and low-oxygen conditions enhance the regenerative potential of perivascular stem cells. *Tissue Eng Part A* 2011;17(1–2):37–44.
- [32] Vorotnikova E, McIntosh D, Dewilde A, Zhang J, Reing JE, Zhang L, et al. Extracellular matrix-derived products modulate endothelial and progenitor cell migration and proliferation in vitro and stimulate regenerative healing in vivo. *Matrix Biol* 2010;29(8):690–700.
- [33] Agrawal V, Tottey S, Johnson SA, Freund JM, Siu BF, Badyal SF. Recruitment of progenitor cells by an extracellular matrix cryptic peptide in a mouse model of digit amputation. *Tissue Eng Part A* 2011;17(19–20):2435–43.
- [34] Agrawal V, Siu BF, Chao H, Hirschi KK, Raborn E, Johnson SA, et al. Partial characterization of Sox2+ cell population in an adult murine model of digit amputation. *Tissue Eng Part A*. <http://dx.doi.org/10.1089/ten.tea.2011.0550>. Available at: <http://www.ncbi.nlm.nih.gov/pubmed/22530556>; 2012.
- [35] Singelyn JM, Sundaramurthy P, Johnson TD, Schup-Magoffin PJ, Hu DP, Faulk DM, et al. Catheter-deliverable hydrogel derived from decellularized ventricular extracellular matrix increases endogenous cardiomyocytes and preserves cardiac function post-myocardial infarction. *J Am Coll Cardiol* 2012;59(8):751–63.
- [36] Sellaro TL, Ranade A, Faulk DM, McCabe GP, Dorko K, Badyal SF, et al. Maintenance of human hepatocyte function in vitro by liver-derived extracellular matrix gels. *Tissue Eng Part A* 2010;16(3):1075–82.
- [37] Tottey S, Johnson SA, Crapo PM, Reing JE, Zhang L, Jiang H, et al. The effect of source animal age upon extracellular matrix scaffold properties. *Biomaterials* 2011;32(1):128–36.
- [38] Cheng MH, Uriel S, Moya ML, Francis-Sedlak M, Wang R, Huang JJ, et al. Dermis-derived hydrogels support adipogenesis in vivo. *J Biomed Mater Res A* 2010;92(3):852–8.
- [39] Hong Y, Takanari K, Amoroso NJ, Hashizume R, Brennan-Pierce EP, Freund JM, et al. An elastomeric patch electrospun from a blended solution of dermal extracellular matrix and biodegradable polyurethane for rat abdominal wall repair. *Tissue Eng Part C Methods* 2012;18(2):122–32.
- [40] Uriel S, Labay E, Francis-Sedlak M, Moya ML, Weichselbaum RR, Ervin N, et al. Extraction and assembly of tissue-derived gels for cell culture and tissue engineering. *Tissue Eng Part C Methods* 2009;15(3):309–21.
- [41] Uriel S, Huang JJ, Moya ML, Francis ME, Wang R, Chang SY, et al. The role of adipose protein derived hydrogels in adipogenesis. *Biomaterials* 2008;29(27):3712–9.
- [42] Stankus JJ, Freytes DO, Badyal SF, Wagner WR. Hybrid nanofibrous scaffolds from electrospinning of a synthetic biodegradable elastomer and urinary bladder matrix. *J Biomater Sci Polym Ed* 2008;19(5):635–52.
- [43] Stuart K, Panitch A. Influence of chondroitin sulfate on collagen gel structure and mechanical properties at physiologically relevant levels. *Biopolymers* 2008;89(10):841–51.
- [44] Chandran PL, Barocas VH. Deterministic material-based averaging theory model of collagen gel micromechanics. *J Biomech Eng* 2007;129(2):137–47.
- [45] Berry CC, Shelton JC, Lee DA. Cell-generated forces influence the viability, metabolism and mechanical properties of fibroblast-seeded collagen gel constructs. *J Tissue Eng Regen Med* 2009;3(1):43–53.
- [46] Bryant SJ, Anseth KS. Hydrogel properties influence ECM production by chondrocytes photoencapsulated in poly(ethylene glycol) hydrogels. *J Biomed Mater Res* 2002;59(1):63–72.
- [47] Engler AJ, Griffin MA, Sen S, Bonnemann CG, Sweeney HL, Discher DE. Myotubes differentiate optimally on substrates with tissue-like stiffness: pathological implications for soft or stiff microenvironments. *J Cell Biol* 2004;166(6):877–87.
- [48] Mio T, Adachi Y, Romberger DJ, Ertl RF, Rennard SI. Regulation of fibroblast proliferation in three-dimensional collagen gel matrix. *In Vitro Cell Dev Biol Anim* 1996;32(7):427–33.
- [49] Saha K, Keung AJ, Irwin EF, Li Y, Little L, Schaffer DV, et al. Substrate modulus directs neural stem cell behavior. *Biophys J* 2008;95(9):4426–38.
- [50] Wall ST, Yeh CC, Tu RY, Mann MJ, Healy KE. Biomimetic matrices for myocardial stabilization and stem cell transplantation. *J Biomed Mater Res A* 2010;95(4):1055–66.
- [51] Brown BN, Ratner BD, Goodman SB, Amar S, Badyal SF. Macrophage polarization: an opportunity for improved outcomes in biomaterials and regenerative medicine. *Biomaterials* 2012;33(15):3792–802.
- [52] Johnson TD, Lin SY, Christman KL. Tailoring material properties of a nanofibrous extracellular matrix derived hydrogel. *Nanotechnology* 2011;22(49):494015.
- [53] Singelyn JM, Christman KL. Modulation of material properties of a decellularized myocardial matrix scaffold. *Macromol Biosci* 2011;11(6):731–8.